Radiative charge transfer and radiative association in $He^+ + Ne$ collisions

X. J. Liu,[1] Y. Z. Qu,[2,*] B. J. Xiao,[1] C. H. Liu,[3] Y. Zhou,[2] J. G. Wang,[3] and R. J. Buenker[4]

[1]*Institute of Plasma Physics, Chinese Academy of Sciences, Hefei 230031, People's Republic of China*

[2]*College of Material Sciences and Optoelectronic Technology, Graduate University of the Chinese Academy of Sciences, Beijing 100049, People's Republic of China*

[3]*Institute of Applied Physics and Computational Mathematics, Beijing 100088, People's Republic of China*

[4]*Fachbereich C-Mathematik und Naturwissenschaften, Bergische Universität Wuppertal, D-42097 Wuppertal, Germany*

(Received 5 November 2009; published 19 February 2010)

A fully quantum-mechanical approach is utilized to study the collision process of He^+ with neutral neon, and the radiative charge transfer (RCT) and radiative association (RA) cross sections are presented in the energy range from 0.08 meV to 1 eV, while the optical potential and semiclassical methods are adopted to calculate the total radiative decay cross sections for energies from 0.08 meV to 5 keV. The potential energy curves and dipole transition matrix elements are obtained by an ab initio multireference configuration interaction package. For the related three lowest $X\,^2\Sigma^+$, $A\,^2\Pi$, and $B\,^2\Sigma^+$ states, the spectroscopic data are in good agreement with other theoretical calculations and experimental measurements. Our results indicate that the RCT cross section is much larger than the nonradiative charge transfer cross section for collision energy $E < 20$ eV, and when $E > 40$ eV, the nonradiative process becomes dominant. Especially, we found that in the present collision system the RA process is more important than the RCT process when $E < 1$ meV. The RCT and RA rate coefficients are also given for temperatures from 1 to 4×10^3 K.

DOI: 10.1103/PhysRevA.81.022717 PACS number(s): 34.70.+e, 34.20.−b

I. INTRODUCTION

The investigation of ion-atom collisions is important not only for fundamental physical research, but also in applied fields such as astrophysics, radiology, and ion-beam interactions with surfaces for ion implantation and thin-film manufacturing. In many plasma environments, such as in the tokomak and interstellar space, He^+ is known to be abundant, and the electron-capture processes in collision with other rare gas-atoms may play a role in the ionization balance and energy transfer. A number of studies aimed at understanding these dynamical processes have been performed [1–4]. These efforts have focused on measurements and calculations of direct charge transfer in the energy region from tens of eV to keV where the nonradiative charge transfer dominates. However, cross sections for nonradiative charge transfer rapidly decrease with decreasing energy, and the radiative decay process becomes dominant in the sub-eV energy region. In order to simulate the low-temperature plasmas consisting of helium ions and neutral neon atoms, it is necessary to provide accurate collision cross sections for radiative decay processes including radiative charge transfer and radiative association.

In this work, we report a theoretical investigation on the radiative charge transfer (RCT) process,

$$He^+(^2S) + Ne(^1S) \rightarrow He(^1S) + Ne^+(^2P) + \hbar\omega, \qquad (1)$$

and the radiative association (RA) process,

$$He^+(^2S) + Ne(^1S) \rightarrow HeNe^+(X^2\Sigma, A^2\Pi) + \hbar\omega. \qquad (2)$$

The corresponding nonradiative charge transfer (nRCT) process is

$$He^+(^2S) + Ne(^1S) \rightarrow He(^1S) + Ne^+(^2P). \qquad (3)$$

The three processes in Eqs. (1)–(3) can be regarded as transitions from the $B\,^2\Sigma^+$ state of the $HeNe^+$ molecular ion to the $X\,^2\Sigma^+$ and $A\,^2\Pi$ states. The radiative charge transfer and radiative association cross sections are calculated by a fully quantum-mechanical approach, while the total radiative decay cross sections are calculated by the optical potential and semiclassical methods. The relevant adiabatic molecular potentials and dipole matrix elements are obtained by the multireference single- and double-excitation configuration interaction (MRD-CI) method [5–8].

The article is organized as follows. In Sec. II we briefly outline the theoretical methods used in the molecular structure and cross-section calculations. In Sec. III we present the results of total radiative decay cross sections, radiative charge transfer, and radiative association for processes (1) and (2), and in Sec. IV we give our conclusions. Atomic units will be used in the remaining part of this article, unless explicitly indicated otherwise.

II. THEORETICAL METHODS

A. Molecular structure calculations

The adiabatic potential energies and molecular electronic wave functions of the $HeNe^+$ system are obtained by employing the multireference single- and double-excitation configuration interaction (MRD-CI) method [5–8] with configuration selection at a threshold of 2×10^{-8} hartree and energy extrapolation using the TABLE-CI algorithm. In the calculations, a basis set of aug-cc-pVTZ (augmented correlation consistent polarization valence triple zeta), that is, (7*s*,3*p*,2*d*) contracted to [4*s*,3*p*,2*d*] for helium [9] and (11*s*,6*p*,3*d*,2*f*) contracted to [5*s*,4*p*,3*d*,2*f*] for neon [10] is employed. The potential and dipole transition matrix elements were calculated from the internuclear distance $R = 1.0$–50 a.u.

*yzqu@gucas.ac.cn

TABLE I. Asymptotic energy levels for the $HeNe^+$ system.

Asymptotic atomic states	Molecular states		Energy (eV) This work	Theory [11]	Experiment (NIST) [12]
$Ne^+(2p^5\,^2P) + He(^1S)$	$1\,^2\Sigma^+ (X\,^2\Sigma^+)$	$1\,^2\Pi (A\,^2\Pi)$	−3.125	−2.930	−3.023
$Ne(^1S) + He^+(1s\,^2S)$	$2\,^2\Sigma^+ (B\,^2\Sigma^+)$		0.000	0.000	0.000
$Ne(2p^5 3s\,^3P) + He^+(1s\,^2S)$	$3\,^2\Sigma^+$	$2\,^2\Pi$	16.732	16.67	16.647

The five adiabatic potential curves, $X\,^2\Sigma^+$, $A\,^2\Pi$, $B\,^2\Sigma^+$, $2\,^2\Pi$, and $3\,^2\Sigma^+$, are plotted as a function of the internuclear distance R in Fig. 1. The two electronic states, $1\,^2\Sigma^+ (X\,^2\Sigma^+)$ and $1\,^2\Pi$ $(A\,^2\Pi)$, are formed in the approach of $Ne^+(^2P^o)$ with $He(^1S)$, the state $2\,^2\Sigma^+$ $(B\,^2\Sigma^+)$ by $Ne(^1S)$ with He^+ (^2S), and the state $3\,^2\Sigma^+$ and $2\,^2\Pi$ by $Ne(2p^5 3s\,^3P)$ and He^+ $(1s\,^2S)$. The calculated asymptotic energies calculated with MRD-CI are presented in Table I. Good agreement is obtained with the available theoretical results and the experimental measurements [11,12]. The maximum relative errors of the current results from the experiment data are less than 4%, and the comparison of our calculated spectroscopic constants with the available theoretical calculations and experimental measurements are displayed in Table II. The results agree well with each other except for the ground state $X\,^2\Sigma^+$. The previously calculated [13,14] and present equilibrium bond length R_e and bond dissociation energy D_e for the $X\,^2\Sigma^+$ state are much closer with one another than the experimental values, so the molecular constants reported in Ref. [15] for the $X\,^2\Sigma$ state need to be revised. Our calculations are consistent with the recommended spectroscopic constants for the $X\,^2\Sigma^+$ state: $R_e = 1.43 \pm 0.01$ Å and $D_e = 5200 \pm 200$ cm^{-1} by Seong *et al.* [14].

Beyond $R = 50$ a.u., the potential curve for the entrance channel $B\,^2\Sigma^+$ is described by the long-range form

$$V_L(R) = -\frac{1}{2}\left(\frac{\alpha_1}{R^4} + \frac{\alpha_2}{R^6} + \frac{\alpha_3}{R^8}\right), \tag{4}$$

where α_1, α_2, and α_3 are the dipole, quadrupole, and octupole polarizabilities of the $Ne(^1S)$ atoms, respectively, which are chosen to be 2.669, 7.518, and 42.07 a.u., respectively [16]. For the final states $X\,^2\Sigma^+$ and $A\,^2\Pi$, the form of the long-range potential is $V_L(R) = -(1/2)(\alpha_d/R^4)$, where $\alpha_d = 1.383$ a.u. [17] is the dipole polarizability of the He (^1S) atoms.

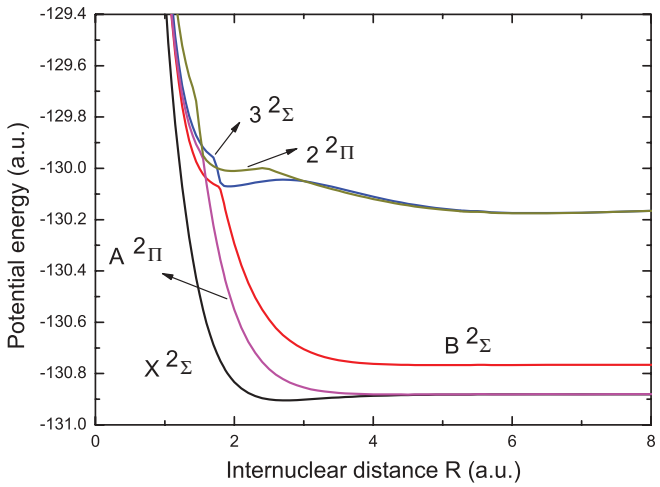

FIG. 1. (Color online) Potential energy curves for the $X\,^2\Sigma^+$, $A\,^2\Pi$, $B\,^2\Sigma^+$, $2\,^2\Pi$, and $3\,^2\Sigma^+$ states.

The dipole matrix elements $D(R)$ from the initial state $B\,^2\Sigma^+$ to the two final states $X\,^2\Sigma^+$ and $A\,^2\Pi$ are presented as a function of R in Fig. 2. The matrix elements are larger for transitions between molecular states of the same symmetry than for transitions between states of different symmetries. There is a slight lack of smoothness in Fig. 2 resulting from the strong nonadiabatic interactions near the avoided crossing positions between $A\,^2\Pi$ or $B\,^2\Sigma^+$ and the upper states [11]. There is an avoided crossing at $R = 1.79$ between $B\,^2\Sigma^+$ and the higher $3\,^2\Sigma^+$ state, resulting in the potential curve of the $B\,^2\Sigma^+$ state far from the $X\,^2\Sigma^+$ but close to the $3\,^2\Sigma^+$ near the crossing position, so that the overlapping of the $X\,^2\Sigma^+$ and $B\,^2\Sigma^+$ states decreases and the dipole matrix element in Fig. 2 decreases dramatically. For the $A\,^2\Pi$ state, there exists another avoided crossing between $A\,^2\Pi$ and $2\,^2\Pi$ at $R = 1.55$ a.u. The strong nonadiabatic interaction near the avoided crossing positions leads to the structure of dipole matrix in Fig. 2. Furthermore, it should be mentioned that the long-range asymptotic behavior of $D(R)$ is fitted to the form $\frac{d_0}{R^n}$.

B. Radiative decay calculations

Both the radiative charge transfer and radiative association processes in Eqs. (1) and (2) can be regarded as a spontaneous radiative decay from a molecular state (i.e., $B\,^2\Sigma^+$) for the ion-atom collision system. They can be treated by an optical potential method that has been described in detail by Zygelman and Dalgarno [18] and successfully applied to calculations of some systems [19–23]. Here we only outline the optical potential method and relevant formulas. During the ion-atom collisions, the transition probability per unit time (i.e., the Einstein coefficient) is represented by the imaginary part of a complex optical potential. The scattering wave $F_a(\vec{R})$, where

TABLE II. Comparison of the equilibrium bond lengths and dissociation energies for the $X\,^2\Sigma^+$, $A\,^2\Pi$, and $B\,^2\Sigma^+$ states of $HeNe^+$.

Molecular states	Spectroscopic constant	This work	Theory [13]	Theory [14]	Experiment [15]
$1\,^2\Sigma^+ (X\,^2\Sigma^+)$	R_e (Å)	1.431	1.427	1.433	1.30
	D_e (cm^{-1})	5221	4979	5452	6216 ± 300
$1\,^2\Pi (A\,^2\Pi)$	R_e (Å)	2.385	2.336	2.441	2.319
	D_e (cm^{-1})	278	363	279	347
$2\,^2\Sigma (B\,^2\Sigma^+)$	R_e (Å)	2.650	2.655	2.639	2.648
	D_e (cm^{-1})	239	356	380	364

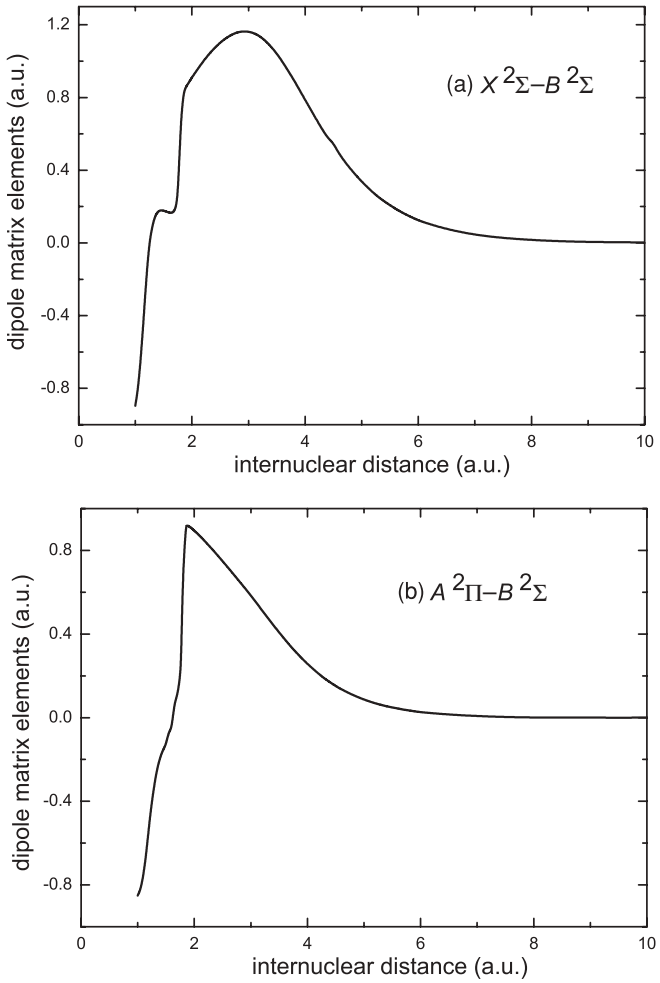

FIG. 2. Dipole matrix elements for the radiative transitions from the initial state $B\,^2\Sigma^+$ to the two final states (a) $X\,^2\Sigma^+$ and (b) $A\,^2\Pi$.

R is the internuclear distance and the subscript a denotes the initial upper molecular state (i.e., $B\,^2\Sigma^+$), is obtained by solving [18]

$$\left[-\frac{1}{2\mu}\nabla^2_{\vec{R}} + V_a(R) - E\right] F_a(\vec{R}) = \frac{i}{2}A(R)F_a(\vec{R}), \tag{5}$$

where E is the relative collision energy in the center-of-mass frame, μ is the reduced mass, $V_a(R)$ is the adiabatic potential energy for the initial upper molecular state a (i.e., $B\,^2\Sigma^+$), and $A(R)$ is the transition probability per unit time for the radiative transition given by

$$A(R) = \frac{4}{3}D^2(R)\frac{|V_a(R) - V_b(R)|^3}{c^3}, \tag{6}$$

where c is the speed of light and $V_b(R)$ is the adiabatic potential energy for the low-lying molecular state b (i.e., $X\,^2\Sigma^+$ and $A\,^2\Pi$ in this work). The cross section for radiative decay (including radiative association and radiative charge transfer) in the collisions can be written as

$$\sigma(E) = \frac{\pi}{k_a^2}\sum_J^\infty (2J+1)[1 - \exp(-4\eta_J)], \tag{7}$$

where η_J is the imaginary part of the phase shift of the Jth partial wave of the radial Schrödinger equation which is given in the distorted-wave approximation by

$$\eta_J = \frac{\pi}{2}\int_0^\infty dR\left|f_J^a(k_aR)\right|^2 A(R), \tag{8}$$

where $k_a = \sqrt{2\mu\,[E - V_a(\infty)]}$, and $f_J^a(k_aR)$ is the regular solution of the homogeneous radial equation

$$\left\{\frac{d^2}{dR^2} - \frac{J(J+1)}{R^2} - 2\mu\,[V_a(R) - V_a(\infty)] + k_a^2\right\} f_J^a(k_aR) = 0, \tag{9}$$

and normalized asymptotically according to

$$f_J^a(k_aR) = \sqrt{\frac{2\mu}{\pi k_a}}\sin\left(k_aR - \frac{J\pi}{2} + \delta_J^a\right). \tag{10}$$

Replacing the summation in Eq. (7) and applying the JWKB approximation, one obtains the expression for the semiclassical cross section

$$\sigma(E) = 2\pi\sqrt{\frac{2\mu}{E}}\int pdp\int_{R_a^{\rm ctp}}^\infty dR\frac{A(R)}{\sqrt{1 - V_a(R)/E - p^2/R^2}}, \tag{11}$$

where p is the impact parameter and $R_a^{\rm ctp}$ is the classical turning point in the incoming channel.

C. Radiative charge transfer and radiative association calculations

In the present work, we use the fully quantum-mechanical approach to calculate the radiative charge transfer [18,21] and radiative association cross sections [24,25]. The radiative charge transfer cross section is given by

$$\sigma = \int_{\omega_{\rm min}}^{\omega_{\rm max}}\frac{d\sigma}{d\omega}d\omega, \tag{12}$$

and

$$\frac{d\sigma}{d\omega} = \frac{8}{3}\left(\frac{\pi}{k_a}\right)^2\frac{\omega^3}{c^3}\sum_J\left[S_J^R(\Delta\Lambda)M^2_{J,J-1}(k_a,k_b) + S_J^Q(\Delta\Lambda)M^2_{J,J}(k_a,k_b) + S_J^P(\Delta\Lambda)M^2_{J,J+1}(k_a,k_b)\right], \tag{13}$$

where ω is the angular frequency of the emitted photon, c is the speed of light, and J is the angular momentum quantum number

$$M_{J,J'}(k_a,k_b) \equiv \int_0^\infty dR f_J(k_aR)D(R)f_{J'}(k_bR). \tag{14}$$

In the above expression, $k_{\rm b} = \sqrt{2\mu\,[E - V_b(\infty) - \hbar\omega]}$ and $S_J^X(\Delta\Lambda)$ where X is R, Q, or P represents the Hönl-london factor [22,26].

The radiative association cross sections can be obtained by subtracting the radiative charge transfer part from the total radiative decay cross sections [19,26]. It can also be calculated directly as

$$\sigma = \sum_J\sum_n\sigma_J(\nu_n), \tag{15}$$

where $\sigma_J(\nu_n)$ is the cross section for a transition from a state of angular momentum J into a vibrational level ν_n in which a

photon of angular frequency ω is emitted. If E_n is the energy of level v_n and E_n is negative, $\hbar\omega = E + \Delta E - E_n$. The partial cross section $\sigma_J(v_n)$ for radiative association into vibration level v_n may be written as

$$\sigma_J(v_n) = \frac{8}{3}\left(\frac{\pi}{k}\right)^2 \frac{1}{c^3}\sum_J \left[\omega^3_{n,J-1} S^R_J(\Delta\Lambda) M^2_{J,J-1}(k_a,k_b) + \omega^3_{n,J} S^Q_J(\Delta\Lambda) M^2_{J,J}(k_a,k_b) + \omega^3_{n,J+1} S^P_J(\Delta\Lambda) M^2_{J,J+1}(k_a,k_b)\right], \quad (16)$$

and

$$M_{J,J'n} \equiv \int_0^\infty dR f_J(R) D(R) \phi^n_{J'}(R), \quad (17)$$

and the vibrational wave function $\phi^n_{J'}(R)$ is the regular solution of the homogenous radial equation

$$\left\{\frac{d^2}{dR^2} - \frac{J'(J'+1)}{R^2} - 2\mu\left[V_b(R) - V_b(\infty) - E_n\right]\right\}\phi^n_{J'}(R) = 0. \quad (18)$$

III. RESULTS AND DISCUSSIONS

A. Cross section for radiative decay

Using the optical potential method described above, we calculated the total radiative decay (including the radiative charge transfer and radiative association) cross sections for collision energies between 0.08 meV and 0.5 eV for the transitions $B\,^2\Sigma^+$–$X\,^2\Sigma^+$ and $B\,^2\Sigma^+$–$A\,^2\Pi$, respectively. The contributions from the individual partial waves are summed in Eq. (7) until convergence of the cross section is achieved. In order to extend the treatment to higher energy, we have also performed a semiclassical calculation using Eq. (11) for the relative energy region from 0.01 eV to 5 keV. The cross sections are displayed in Fig. 3. In the overlapping energy range of 0.01–0.5 eV, except the shape resonance behavior, the semiclassical cross sections are in agreement with the optical potential results. The resonant structures, appearing in the energy region 10^{-4}–0.02 eV, are attributed to the presence of quasibound or virtual rotational-vibrational levels in the entrance channel [21–23]. In the semiclassical approach, no quasibound or virtual rotational-vibrational levels exist. Thus, the semiclassical approximation is believed to be able to give reliable cross sections in the higher energy region. For large energies ($E \gg V_a$), the double integral in Eq. (11) is nearly energy independent and therefore $\sigma(E)$ varies as $1/\sqrt{E}$. The numerical results for all the transitions display such behavior for $E \geqslant 30$ eV.

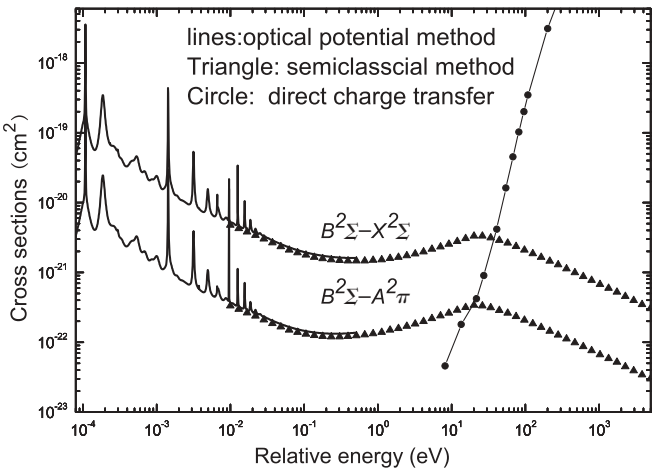

FIG. 3. Cross sections for radiative decay to the $X\,^2\Sigma^+$ and $A\,^2\Pi$ states from the $B\,^2\Sigma^+$ state in $He^+ + Ne$ collisions. Radiative decay cross sections are obtained by the optical potential method (lines) and the semiclassical method (triangle), respectively, and direct charge transfer cross sections are the results of Zygelman and Dalgarno [3] (circles).

The diagram in Fig. 3 illustrates rich resonance structures in the energy region between 0.1 meV and 0.02 eV. It is obvious that resonances for transitions with the same initial molecular states should appear in the same positions. The resonances may give rise to enhancement in the rate coefficients. For these two transitions, the background cross section, excluding resonances, decreases monotonically as the relative collision energy increases from 0.08 meV to 0.5 eV. However, when the relative energy increases continuously, the semiclassical cross sections ascend gradually until reaching a maximum at ~20 eV and then decrease as $1/\sqrt{E}$. This behavior can be understood from the potential curves and transition probabilities. For the initial state $B\,^2\Sigma^+$, the corresponding classical turning point $R_a^{\rm ctp}$ is less than 4.0 a.u. when the relative energy is more than 0.5 eV, as shown in Fig. 1. The transition probability $A(R)$ in Eq. (6), which is displayed in Fig. 4, increases rapidly as R decreases, so that the integral in Eq. (11) increases faster than the factor of $1/\sqrt{E}$ as the collision energy increases and the $R_a^{\rm ctp}$ decreases, resulting in an increasing tendency for the cross section. When the relative energy is more than 30 eV, the classical turning point $R_a^{\rm ctp}$is less than 1.5 a.u. Thereafter, $A(R)$ tends toward zero and the integral in Eq. (11) does not increase further and $\sigma(E)$varies as $1/\sqrt{E}$. From Fig. 4, we can also see that the transition probabilities for $B\,^2\Sigma^+$–$X\,^2\Sigma^+$ are almost one order of magnitude larger than that for $B\,^2\Sigma^+$–$A\,^2\Pi$. Therefore, the radiative decay cross section for the $B\,^2\Sigma^+$–$X\,^2\Sigma^+$ transition is one order of magnitude larger than for the $B\,^2\Sigma^+$–$A\,^2\Pi$ transition, as shown in Fig. 3.

In Fig. 3, we also compare the present radiative decay cross sections with the nonradiative charge transfer cross sections of Zygelman and Dalgarno [3] calculated using a model-potential method. As the collision energy increases, the nonradiative charge transfer cross sections increase rapidly. When $E > 40$ eV, the nonradiative process becomes the dominant charge transfer mechanism.

B. Cross section for radiative charge transfer and radiative association

The fully quantum-mechanical approach has been used to describe the radiative charge transfer and radiative association in the $He^+ + Ne$ collisions, and the cross sections are displayed in Figs. 5(a) and 5(b) for the $B\,^2\Sigma^+$–$X\,^2\Sigma^+$ and $B\,^2\Sigma^+$–$A\,^2\Pi$ transitions, respectively. In Fig. 5(a), the association process is seen to be more important than the charge transfer: the radiative charge transfer cross sections are about 1/4 of the radiative association cross sections at energies from 0.08 meV–0.05 eV. As the collision energy

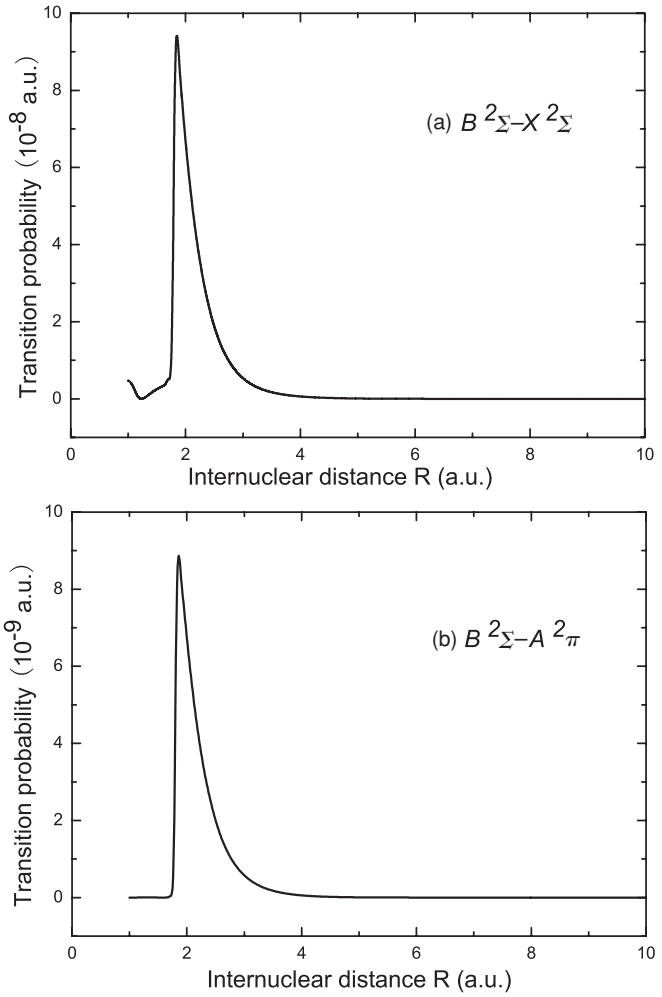

FIG. 4. Transition probabilities (a) for $B\,^2\Sigma^+$–$X\,^2\Sigma^+$ and (b) for $B\,^2\Sigma^+$–$A\,^2\Pi$.

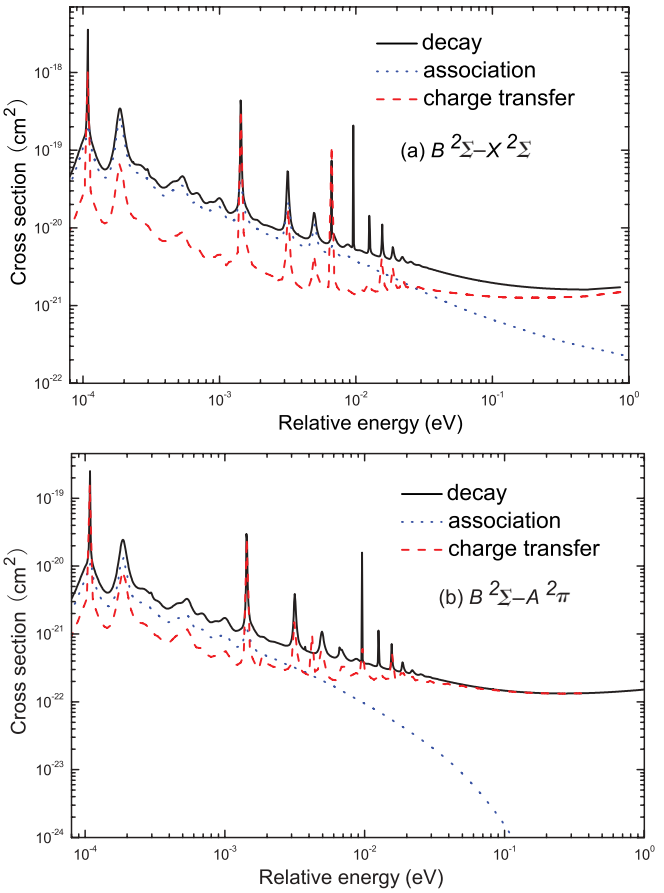

FIG. 5. (Color online) The radiative association (dotted line), radiative charge transfer (dashed line), and total radiative decay (solid line) cross sections in the $He^+ + Ne$ collisions for (a) $B\,^2\Sigma^+$–$X\,^2\Sigma^+$ transitions and (b) $B\,^2\Sigma^+$–$A\,^2\Pi$ transitions.

increases, the difference between the radiative association and charge transfer cross sections decreases. The radiative association cross sections decrease more rapidly than that of the radiative charge transfer. This is because of the fact that the effective angular momentum quantum numbers increase with collision energy, and this results in a shallower well of the effective potential $V_J^{\rm eff}(R) = V(R) + \frac{J(J+1)}{2\mu R^2}$ for the final state, causing the number of the quasibound vibrational levels to become smaller. For the $B\,^2\Sigma^+$–$A\,^2\Pi$ transition in Fig. 5(b), the radiative charge transfer cross sections are about twice as large as the radiative association cross sections in the energy range of 0.08 ∼ 10 meV. When the energy is more than 10 meV, the radiative association cross sections decrease sharply, so that the radiative charge transfer becomes the dominant contributor to the total radiative decay. Besides, we can see that the association for $B\ ^2\Sigma^+$–$X\ ^2\Sigma^+$ is more important than that for $B\,^2\Sigma^+$–$A\,^2\Pi$. This is because the $X\,^2\Sigma^+$ ground state has a deeper well (∼0.65 eV) than the $A\,^2\Pi$ state, and thus more quasibound vibrational levels can be formed.

In the present system of interest, due to the strong adsorbability of inert gas ions, He^+ and neutral Ne can form a $HeNe^+$ molecule easily at low energy, and this characteristic is different from the case in the previous work [27,28] for $H^+ + Na$ collisions where the radiative association cross section is much smaller than that of radiative charge transfer. We find that even for the $A\,^2\Pi$ final state with a very shallow well (∼0.035 eV), the contribution from radiative association to total radiative decay is important and cannot be neglected. This difference is produced by the dipole matrix elements. As shown in Fig. 2, the dipole matrix elements for the $He^+ + Ne$ system are compact and located within $R < 10$ a.u. for the $B\,^2\Sigma^+$–$X\,^2\Sigma^+$ transition and $R < 8$ for the $B\,^2\Sigma^+$–$A\,^2\Pi$ transition, respectively, while for the $H^+ + Na$ system [27,28], the dipole matrix element is diffuse up to a large internuclear distance until $R \sim 20$ a.u. The radiative association transition matrix elements $M_{J,J'n}$ in Eq. (18) depend on the overlapping of the vibrational wave functions and dipole matrix elements. For the $He^+ + Ne$ system, the overlapping is more effective, resulting in a larger radiative association cross section, so that the radiative association dominates over the radiative charge transfer process at low energy.

There is another independent procedure available for the radiative association process, as described by Zygelman *et al.* [19], namely to obtain the cross sections by subtracting the radiative charge transfer part from the total radiative decay cross sections. For low energies, the results from the two methods are in agreement with each other (e.g., at 1 meV the two results differ by less than 4%). However, as the collision

TABLE III. Comparison of the total decay cross sections obtained by the optical potential and the fully quantum-mechanical methods for both of the $B\,^2\Sigma$–$X\,^2\Sigma$ and $B\,^2\Sigma$–$A\,^2\Pi$ transitions.

Energy (meV)	Total decay cross sections (in cm^2)	RCT + RA cross sections (in cm^2)	Relative error
	$B\,^2\Sigma$–$X\,^2\Sigma$		
0.1	1.352[−19][a]	1.341[−19]	0.8%
0.5	4.136[−20]	4.028[−20]	2.6%
1.0	2.418[−20]	2.334[−20]	3.5%
5.0	1.475[−20]	1.513[−20]	2.6%
10	5.228[−21]	4.830[−21]	7.6%
50	2.511[−21]	2.620[−21]	4.4%
100	1.964[−21]	1.914[−21]	2.5%
500	1.610[−21]	1.567[−21]	2.7%
1000	1.761[−21]	1.640[−21]	6.9%
	$B\,^2\Sigma$–$A\,^2\Pi$		
0.1	9.704[−21]	9.364[−21]	3.5%
0.5	2.950[−21]	2.794[−21]	5.3%
1.0	1.725[−21]	1.555[−21]	9.8%
5.0	1.023[−21]	0.981[−21]	4.1%
10	3.683[−22]	3.982[−22]	8.1%
50	1.799[−22]	1.814[−22]	0.8%
100	1.462[−22]	1.449[−22]	0.8%
500	1.372[−22]	1.366[−22]	0.5%
1000	1.516[−22]	1.477[−22]	2.5%

[a]The number in square brackets denotes the power of 10; i.e., $A[B] = A \times 10^B$.

energy increases, the discrepancy becomes larger since the radiative association cross sections decrease rapidly, causing the cross section difference between the total radiative decay and radiative charge transfer to be less reliable. In Table III, we compare the total decay cross sections obtained by the optical potential and fully quantum-mechanical methods for both the $B\,^2\Sigma$–$X\,^2\Sigma$ and $B\,^2\Sigma$– $A\,^2\Pi$ transitions in the energy region of $10^{-4} \sim 1$ eV. It is found that the two results are in good agreement within an error of less than 10%. By comparing the DW results with the fully quantum-mechanical calculations, it is found that the DW approximation is reasonable above 10^{-4} eV.

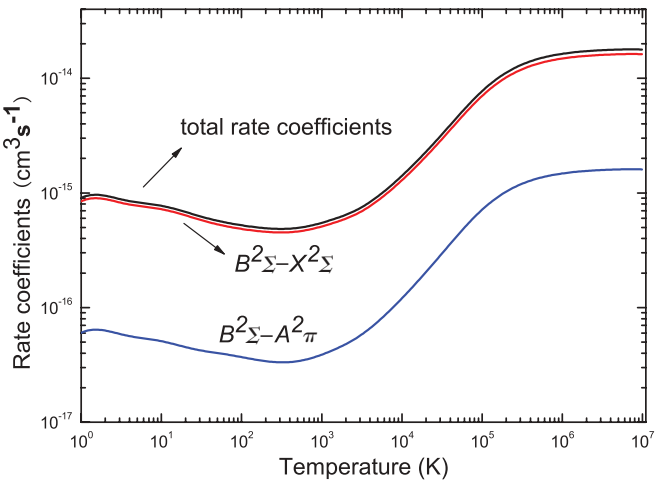

FIG. 6. (Color online) Radiative decay rate coefficients as a function of temperature for the $B\,^2\Sigma^+$–$X\,^2\Sigma^+$ and $B\,^2\Sigma^+$–$A\,^2\Pi$ transitions and their summation.

C. Rate coefficients

The radiative decay rate coefficients for the $B\,^2\Sigma^+$–$X\,^2\Sigma^+$ and $B\,^2\Sigma^+$–$A\,^2\Pi$ transitions and their summation are obtained by averaging the radiative decay cross sections in Fig. 3 over a Maxwellian velocity distribution, and they are plotted in Fig. 6 as a function of temperature from 1 to 10^7 K. The rate coefficients from the $B\,^2\Sigma^+$–$X\,^2\Sigma^+$ transitions is one order of magnitude larger than that from the $B\,^2\Sigma^+$–$A\,^2\Pi$ transitions, and this is consistent with the magnitude of the radiative decay cross sections in Fig. 3. Each curve has a minimum value near 300 K and then rapidly increases with increasing temperature. Above 10^6 K, the rate coefficient approaches a constant value, which is caused by the fact that the cross section behaves as $1/\sqrt{E}$ at large energies.

The radiative association and radiative charge transfer rate coefficients are obtained by averaging the cross sections shown in Figs. 5(a) and 5(b) over a Maxwellian velocity distribution,

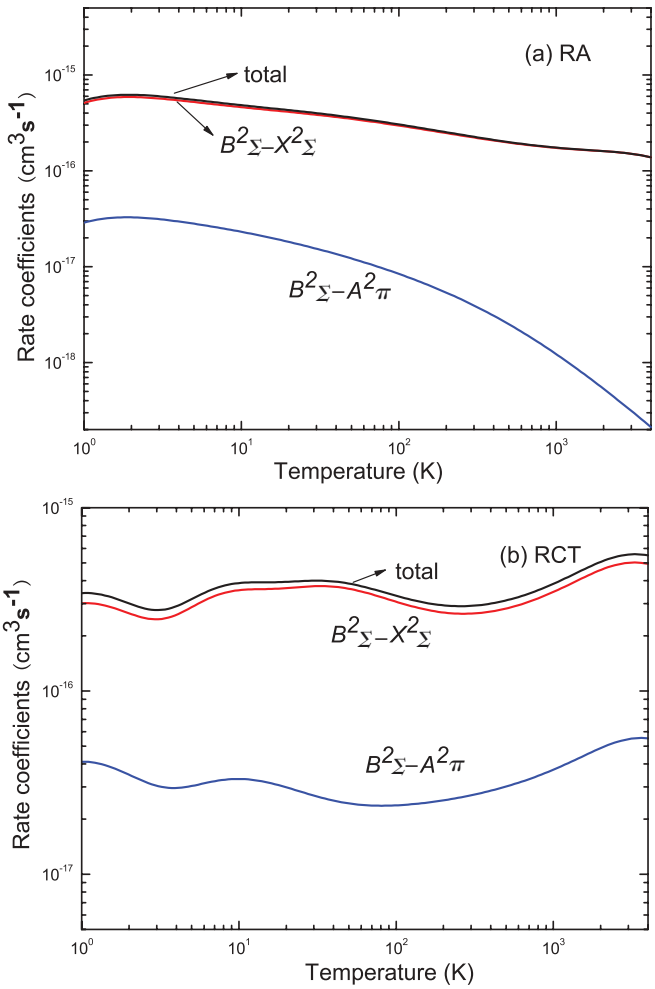

FIG. 7. (Color online) (a) Radiative association (RA) rate coefficients as a function of temperature for the $B\,^2\Sigma^+$–$X\,^2\Sigma^+$ and $B\,^2\Sigma^+$–$A\,^2\Pi$ transitions and their summation. (b) Radiative charge transfer (RCT) rate coefficients as a function of temperature for the $B\,^2\Sigma^+$–$X\,^2\Sigma^+$ and $B\,^2\Sigma^+$–$A\,^2\Pi$ transitions and their summation.

TABLE IV. Fitting parameters of rate coefficients for total radiative decay, radiative association, and radiative charge transfer from the $B\,^2\Sigma^+$ to the $X\,^2\Sigma^+$ and $A\,^2\Pi$ states; a_i and c_i are in units of $cm^3\ s^{-1}$ and K, respectively.

Total decay rate coefficients		Radiative association rate coefficients				Total radiative charge transfer rate coefficients	
		$B\,^2\Sigma$–$X\,^2\Sigma$		$B\,^2\Sigma$–$A\,^2\Pi$			
Parameters	Value	Parameters	Value	Parameters	Value	Parameters	Value
a_1	6.11[−15][a]	a_1	−1.079[−12]	a_1	0.0498[−16]	a_1	1.938[−15]
b_1	0.0498	b_1	0.661	b_1	−0.630	b_1	0.620
c_1	3.145[6]	c_1	0.373	c_1	1.999[3]	c_1	5.755[3]
a_2	−7.720[−15]	a_2	−1.513[−16]	a_2	9.496[−12]	a_2	4.002[−16]
b_2	0.102	b_2	−0.164	b_2	2.725[2]	b_2	0.0002
c_2	1.160[5]	c_2	1.574[4]	c_2	9.350[1]	c_2	1.804[2]
a_3	3.405[−15]	a_3	−1.299[−15]	a_3	−0.0058[−16]	a_3	−9.303[−9]
b_3	0.331	b_3	0.852	b_3	−0.845	b_3	1.992
c_3	3.311[7]	c_3	5.938[2]	c_3	3.884[1]	c_3	1.520

[a]The number in square brackets denotes the power of 10; i.e., $A[B] = A \times 10^B$.

and then plotting them as a function of temperature from 1 to 4000 K [see Figs. 7(a) and 7(b), respectively]. It can be seen that for both the radiative charge transfer and radiative association, the dominant transition is $B\,^2\Sigma^+$–$X\,^2\Sigma^+$, and its cross section is about one order of magnitude larger than for the $B\,^2\Sigma^+$–$A\,^2\Pi$ transition, which is consistent with the data in Fig. 5. When $T > 4000$ K, the contribution from nonradiative processes becomes dominant.

For convenience in applications, the rate coefficients are fitted to the form

$$\alpha(T) = \sum_i a_i \left(\frac{T}{10\,000}\right)^{b_i} \exp\left(-\frac{T}{c_i}\right). \qquad (19)$$

where α is the rate coefficient in $cm^3\ s^{-1}$ and T is temperature in K. The fitting parameters are provided in Table IV. (The units for a_i and c_i are $cm^3\ s^{-1}$ and K, respectively.) The errors in fitting the total decay rate coefficients are within 3% over the temperature range of 3800–10^7 K and less than 8% for 1–3800 K. There are two fitting parameters for radiative association rate coefficients due to the different final states. And the difference between calculation and fitting is less than 3% in the entire temperature range from 1 to 4000 K for the $B\,^2\Sigma^+$–$X\,^2\Sigma^+$ transition; while the fitting is reliable to within 6% from 1–2000 K for the $B\,^2\Sigma^+$–$A\,^2\Pi$ transition, when T is above 2000 K the rate coefficients decrease rapidly, and the fitting is no longer reliable, so that the maximum discrepancy can approach to 50%. However, because the rate coefficients are so small in this range we can effectively ignore this result. At the same time, the fitting for the radiative charge transfer rate coefficients is satisfactory within 4% over the entire temperature region.

IV. CONCLUSION

In the present work, cross sections have been calculated for radiative charge transfer and radiative association due to collisions of He^+ with neutral neon in the energy range from 0.08 to 1 eV by employing a fully quantum-mechanical approach. The optical potential and semiclassical methods were also adopted to calculate the total radiative decay cross sections for energies in the range of 0.08–5 keV. Our results indicate that the RCT cross section is much larger than the nonradiative charge transfer cross section for collision energy $E < 20$ MeV, but that the nonradiative process becomes dominant when $E > 40$ MeV. In particular, we found that in the present collision system the RA process is more important than the RCT process when $E < 1$ meV. The RCT and RA rate coefficients are also given for temperatures between 1 K and 4×10^3 K. In subsequent work, we will focus our interest on the highly excited states of $HeNe^+$ and calculate cross sections for direct charge transfer in the high-energy collision region. The present results will be useful for numerical simulations of low-temperature plasmas.

ACKNOWLEDGMENTS

This work was partially supported by the National Science Foundation of China under Grants No. 10774186 and No. 10835009, NASF under Grant No. 10876043, the Major Direction Fund of Knowledge Innovation Project of the Chinese Academy of Science (Grant No. KJCX3.SYW.N4), and the JSPS-CAS Core-University Program.

[1] F. L. Eisele and S. W. Nagy, J. Chem. Phys. **66**, 883 (1977).
[2] R. Johnsen, Phys. Rev. A **28**, 1460 (1983).
[3] B. Zygelman and A. Dalgarno, Phys. Rev. A **33**, 3853 (1986).
[4] H. Martínez, C. Cisneros, J. de Urquijo, and I. Alvarez, Phys. Rev. A **38**, 5914 (1988).
[5] R. J. Buenker and S. D. Peyerimhoff, Theoret. Chim. Acta. **35**, 33 (1974).

[6] R. J. Buenker and S. D. Peyerimhoff, Theoret. Chim. Acta. **39**, 217 (1975).
[7] R. J. Buenker and R. A. Phillips, J. Mol. Struct., Theochem **123**, 291 (1985).
[8] R. J. Buenker, Int. J. Quantum Chem. **29**, 435 (1986).
[9] D. E. Woon and T. H. Dunning Jr., J. Chem. Phys. **100**, 2975 (1994).
[10] T. H. Dunning Jr., J. Chem. Phys. **90**, 1007 (1989).
[11] R. J. Blint, Phys. Rev. A **14**, 971 (1976).
[12] http://physics.nist.gov/PhysRefData/ASD/levels_form.html; E. B. Saloman and C. J. Sansonetti, J. Phys. Chem. Ref. Data **33**, 1113 (2004); G. W. F. Drake and W. C. Martin, Can. J. Phys. **76**, 679 (1998).
[13] T. G. Wright, B. R. Gray, L. A. Viehland, and R. Johnsen, J. Chem. Phys. **129**, 184307 (2008).
[14] J. Seong, K. C. Janda, M. P. McGrath, and N. Halberstadt, Chem. Phys. Lett. **314**, 501 (1999).
[15] I. Dabrowski and G. Herzberg, J. Mol. Spectrosc. **73**, 183 (1978).
[16] J. Mitroy and J. Y. Zhang, Phys. Rev. A **76**, 032706 (2007).
[17] K. T. Tang and J. P. Toennies, J. Chem. Phys. **118**, 4976 (2003).
[18] B. Zygelman and A. Dalgarno, Phys. Rev. A **38**, 1877 (1988).
[19] B. Zygelman, A. Dalgarno, M. Kimura, and N. F. Lane, Phys. Rev. A **40**, 2340 (1989).
[20] B. W. West, N. F. Lane, and J. S. Cohen, Phys. Rev. A **26**, 3164 (1982).
[21] P. C. Stancil and B. Zygelman, Astrophys. J. **472**, 102 (1996).
[22] L. B. Zhao, P. C. Stancil, J. P. Gu, H.-P. Liebermann, Y. Li, P. Funke, R. J. Buenker, B. Zygelman, M. Kimura, and A. Dalgarno, Astrophys. J. **615**, 1063 (2004).
[23] L. B. Zhao, J. G. Wang, P. C. Stancil, J. P. Gu, H.-P. Liebermann, R. J. Buenker, and M. Kimura, J. Phys. B **39**, 5151 (2006).
[24] B. Zygelman and A. Dalgarno, Astrophys. J. **365**, 239 (1990).
[25] F. A. Gianturco and P. G. Giorgi, Astrophys. J. **479**, 560 (1997).
[26] G. Herzberg, *Molecular Spectra and Molecular Structure*, *Vol. I: Spectra of Diatomic Molecules*, 2nd ed. (Litton, New York, 1950).
[27] C. H. Liu, Y. Z. Qu, Y. Zhou, J. G. Wang, Y. Li, and R. J. Buenker, Phys. Lett. **A373**, 3761 (2009)
[28] C. H. Liu, Y. Z. Qu, Y. Zhou, J. G. Wang, Y. Li, and R. J. Buenker, Phys. Rev. A **79**, 042706 (2009).